Analytica Chimica Acta 706 (2011) 343–348

Contents lists available at SciVerse ScienceDirect

Analytica Chimica Acta

journal homepage: www.elsevier.com/locate/aca

A novel, ultra sensible biosensor built by layer-by-layer covalent attachment of a receptor for diagnosis of tumor growth

Zihni Onur Uygun[a], Mustafa Kemal Sezgintürk[b,*]

[a] Çanakkale Onsekiz Mart University, Faculty of Science, Chemistry Department, Çanakkale, Turkey
[b] Namık Kemal University, Faculty of Science, Chemistry Department, Biochemistry Division, Tekirdağ, Turkey

ARTICLE INFO

Article history:
Received 1 February 2011
Received in revised form 11 August 2011
Accepted 26 August 2011
Available online 3 September 2011

Keywords:
Tumor growth
Cancer
Vascular endothelial growth factor
Vascular endothelial growth factor receptor-1
Electrochemical impedance spectroscopy
Biosensor

ABSTRACT

In the presented research, a novel, ultra sensitive biosensor for the impedimetric detection of vascular endothelial growth factor (VEGF) is introduced. The human vascular endothelial growth factor receptor 1 (VEGF-R1, Flt-1) was used as a biorecognition element for the first time. The immobilization of VEGF-R1 on glassy carbon electrodes was carried out using layer-by-layer covalent attachment of VEGF-R1. The electrochemical properties of the layers constructed on the electrodes were characterized by electrochemical impedance spectroscopy (EIS) and cyclic voltammetry (CV). The differences in electron transfer resistance (R_{et}) between the working solution and the biosensor surface, recorded by the redox probe $K_3[Fe(CN)_6]/K_4[Fe(CN)_6]$, confirmed the binding of VEGF to VEGF-R1. The new biosensor allowed a detection limit of 100 fg mL^{-1} with a linear range of 100–600 fg mL^{-1} to be obtained. The biosensor also exhibited good repeatability (with a correlation coefficient of 1.95%), and reproducibility.

1. Introduction

In the last few decades it has been proved that the role of oncoproteins and other proteins in cancer development is vitally important. The analysis and characterization of these kinds of proteins reveals patterns of cancer and indicates the stage it has reached. Electrochemical biosensors are instruments which analyze a specific biochemical compound using an electrochemical signal that can be detected, amplified and analyzed. Biosensor technologies can be developed to detect emerging cancer biomarkers such as specific proteins circulating in the blood. Further, the biosensors have the potential of providing a rapid, sensitive, and low-cost measurement technology for monitoring angiogenesis and cancer metastasis, and can be used to determine the effectiveness of anti-cancer chemotherapy agents.

Recently, EIS has become an efficient method in many chemical and physical processes. EIS gives analytic solutions for many processes. Besides these, identification of membranes, biosensor characterization and fabrication can also be monitored by EIS effectively. Conversely, enzyme–substrate interactions occurring after antigen–antibody, receptor–ligand or DNA–DNA interactions which have no catalytic reaction, can be successively monitored by EIS [1–3].

The object of the study is to develop an electrochemical biosensor system based on electrochemical impedance spectroscopy which will enable fast, sensitive, and practical determination of a potential cancer biomarker, VEGF, which is a protein produced by cells that stimulates vasculogenesis and angiogenesis In the current study, human vascular endothelial growth factor receptor 1 (VEGF-R1, Flt-1) was used as a biorecognition element for the first time. The recombinant soluble VEGF-R1 binds to VEGF with high affinity [4–6]. Glassy carbon electrodes were coated potentiometrically with thin gold film. Cysteamine monolayers were self-assembled on the gold films. After that, VEGF-R1 was covalently immobilized on the glassy carbon electrodes using an avidin–biotin system. On the basis of cyclic voltammetry and electrochemical impedance investigations, we carried out the immobilization steps. For analyzing the spectrums, EIS data was fitted to an equivalent circuit model. Certain important parameters, such as the DC potential applied to the system, were optimized to obtain the best results. Finally, artificial serum samples spiked with VEGF were analyzed by the biosensor.

2. Experimental

2.1. Materials and instrumentation

All reagents were of analytical grade unless stated otherwise, and were purchased from Sigma–Aldrich (St. Louis, MO, USA). VEGF receptor-1 (Flt-1)/Fc chimera (human) and vascular endothelial

* Corresponding author. Tel.: +90 282 293 38 66; fax: +90 282 293 41 49.
E-mail addresses: msezginturk@hotmail.com, mustafa.kemal.sezginturk@ege.edu.tr, msezginturk@nku.edu.tr (M.K. Sezgintürk).

0003-2670/$ – see front matter © 2011 Elsevier B.V. All rights reserved.
doi:10.1016/j.aca.2011.08.044

growth factor (human) were purchased from Sigma–Aldrich (St. Louis, MO, USA). The contents of the vials were reconstituted using ultra pure water. VEGF-R1 and VEGF portions were prepared at a certain concentrations and were stored at −20 °C until use. Artificial serum solution was prepared by using 4.5 mM KCl, 5 mM $CaCl_2$, 1.6 mM $MgCl_2$, 4.7 mM D(+)-glucose, 2.5 mM urea, 0.1% human serum albumin, and 145 mM NaCl. A three-electrode system, consisting of a gold working electrode, an Ag/AgCl (saturated KCl) reference electrode and a Pt counter electrode, was placed in a 10-mL electrochemical cell (all the electrodes were obtained from iBAS, Warwickshire, UK). Electrochemical experiments were performed using a Compactstat with an integrated impedance analyzer (Ivium Technologies, Eindhoven, The Netherlands) interfaced with a PC. Software designed for conducting physical electrochemistry, pulse voltammetry, and electrochemical impedance spectroscopy was used (Ivium Technologies, Eindhoven, The Netherlands). In all electrochemical experiments a Faraday cage (from iBAS, Warwickshire, UK) was used to block out external static electric fields.

2.2. Preparation of the gold layers and the self-assembled monolayer of cysteamine

Prior to use, the surfaces of the glassy carbon electrodes were polished with 0.05 μm Al_2O_3 powder and then washed ultrasonically in deionized water for 5 min to remove any alumina particles. Afterwards, an electrochemical pre-treatment was carried out using multi cycle voltammetric scanning (30×) between −500 and +500 mV at 0.1 V s^{-1}, in 0.1 M H_2SO_4 solution. The polishing step and electrochemical cleaning were repeated before every electrode preparation step. In order to produce a gold layer on the glassy carbon surface, a potential of −200 mV was applied to an electrode in a gold(III) chloride trihydrate solution (200 ppm, deoxygenated with pure argon gas). Following that the electrode plated with thin gold film was washed with ultra pure water and then it was dried in an argon stream. In the next step, the electrode was immediately immersed in a cysteamine solution (0.1 M, in pure ethanol) for 20 h. After this period, it was rinsed with ethanol and gently dried in an argon stream.

2.3. Immobilization of VEGF-R1 on glassy carbon electrode surfaces

The binding of avidin to a self-assembled monolayer of cysteamine was carried out by combining the amino groups of avidin and cysteamine with glutaraldehyde. For this purpose, first of all a glutaraldehyde solution (25 μL, 2.5%) was spread over the electrode surface, and was then left for 30 min. Then, avidin solution (10 μL, 1 mg mL^{-1}) was added to the glutaraldehyde-modified surface. Two hours later, the avidin-modified electrode was washed by gently immersing the electrode in ultra pure water. Following that, the surface of the electrode was dried in an argon stream. For complexation of avidin–biotin, biotin (10 μL, 1 mg mL^{-1}) solution was dropped on the avidin-modified surface. The incubation period for avidin–biotin complexation was kept constant at 2 h for all experiments. The last step of the immobilization was the binding of VEGF-R1 to biotin. For this, the terminal –COOH group of biotin was used. The activation of this –COOH group was carried out using 1-ethyl-3-(3-dimehylaminopropyl) carbodiimide (EDC)/N-hydroxysuccinimide (NHS) couple. The biotin-modified electrode was dipped in a glass bottle containing EDC/NHS solution (0.04 mM EDC, 0.01 mM NHS) for an hour in a dark ambiance. Later, the electrode was gently washed with ultra pure water, and then it was dried in a pure argon stream again. Immediately afterwards, 10 μL of VEGF-R1 portion was applied to the active electrode surface with a pipette. The electrode was allowed to incubate for 2 h in a moisture medium. Finally, the electrode was immersed into ultra pure water to remove physically adsorbed VEGF-R1 molecules. The glassy carbon electrodes and the modified electrodes were denoted as GCE, GCE/Au, GCE/Au/Cys, GCE/Au/Cys/Avi, GCE/Au/Cys/Avi/Bio, and GCE/Au/Cys/Avi/Bio/VEGF-R1.

2.4. Electrochemical measurements

Cyclic voltammetry was used to characterize the layer-by-layer formation of the biosensors. The potential was varied between 0 and 500 mV (step size: 20 mV, scan rate: 50 mV s^{-1}) in the presence of 5 mM $K_3[Fe(CN)_6]/K_4[Fe(CN)_6]$ (1:1) solution containing 0.1 M KCl. This solution was used as a redox probe in all electrochemical experiments. For electrochemical impedance studies, an alternating wave of 10 mV amplitude was applied to the electrode over the formal potential of the redox couple (0.18 V). The redox couple used for impedance studies was the same as that used in cyclic voltammetry. Impedance spectra were collected in the frequency range between 10,000 and 0.05 Hz.

2.5. Measurement procedure

After each of the VEGF-R1 biosensor was assembled, the biosensor surface was used to interact with the VEGF solution. The standard solution of VEGF was injected over the biosensor surface by a micro-pipette. For each time measurement, the injection volume was 5 μL. The response value was read after 1 h's incubation in a moisture medium. After this incubation period, the biosensor was gently immersed into the ultra pure water ten times to remove physically adsorbed VEGF molecules. Finally, the biosensor was again put into the cell containing the $Fe(CN)_6^{4-/3-}$ redox probe solution and the electrochemical measurements were made as described in the previous section. The difference in charge transfer resistance between the biosensor unbounded and bounded VEGF was used to prepare VEGF calibration curves.

3. Results and discussion

In this study, the VEGF was chosen for detection because it is a specific protein expressed under certain conditions including angiogenesis, tumor growth, metastasis, rheumatoid arthritis, diabetic retinopathy [7,8]. Previously, a number of determination systems for VEGF have been reported. For example, technology using semiconductor nanowire-based sensor systems has been developed for detection of VEGF [9–15]. Lee and coworkers reported label-free and electrical detection of VEGF using anti-VEGF aptamer-modified Si nanowire field-effect transistors [16]. In this method, the synthesis of Si nanowire field-effect transistors was quite difficult. In addition, they reported that the detection limit for VEGF was 1.04 nM and 104 pM. When these molar concentration values were converted to ng mL^{-1}, it can be seen that the detection limits were 40 ng mL^{-1} and 4 ng mL^{-1} for of n-type and p-type SiNW-FETs, respectively. Prabhulkar and coworkers also reported a biosensor based on ferrocene monocarboxylic acid. This was labeled anti-VEGF and was covalently immobilized on a microelectrode surface [17]. The biosensor allowed VEGF analysis with a detection limit of about 38 pg mL^{-1}. However, the immobilization of the VEGF antibodies was based on the electrostatic interaction between the amine and carboxylic groups. In this procedure, an important drawback was the random orientation of VEGF antibodies on carbon fiber electrodes. This random orientation of antibodies could negatively affect the sensitivity of the biosensors [18].

Kim and coworkers also reported an electrochemical method for the detection of VEGF. In this method, gold nanoparticles were self-assembled onto an indium tin oxide electrode. VEGF antibodies were cleaved into half fragments and were then immobilized

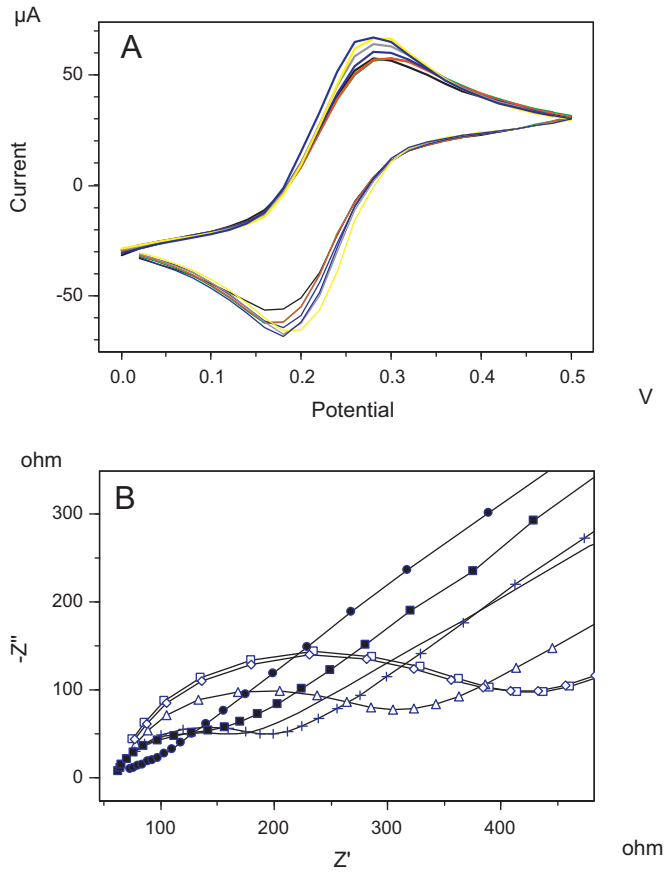

Fig. 1. Electrochemical characterization of the biosensor. (A) Cyclic voltammograms of VEGF-R1 immobilization by layer-by-layer covalently attachment, black: bare GCE; dark blue: GCE/Au; yellow: GCE/Au/Cys; grey: GCE/Au/Cys/Avidin; blue: GCE/Au/Cys/Avidin/Bio; red: GCE/Au/Cys/Avidin/Bio/EDC-NHS; green: GCE/Au/Cys/Avidin/Bio/VEGF-R1. (B) Electrochemical impedance spectrums of VEGF-R1 immobilization steps, straight line: bare GCE; -■-■-: GCE/Au; -●-●-: GCE/Au/Cys; -+-+-: GCE/Au/Cys/Avi; -◊-◊-: GCE/Au/Cys/Avi/Bio; -△-△-: GCE/Au/Cys/Avi/Bio/EDC-NHS; -□-□-: GCE/Au/Cys/Avi/Bio/VEGF-R1. (For interpretation of the references to color in this figure legend, the reader is referred to the web version of the article.)

on gold nanoparticle substrates by their thiol groups [19]. It was reported that VEGF could be analyzed as low as 100 pg mL^{-1} by this technique. In this study, however, there were some situations where it was questionable whether antibody cleavage and purification of fragments should be used in practice. Beside all these techniques we developed a novel biosensor system for ultra sensitive and low-cost detection of VEGF. The results obtained by immobilization, optimization and characterization studies of the biosensor are discussed below.

3.1. Immobilization of VEGF-R1 through layer-by-layer covalent attachment

The layer formation of the biosensors was characterized by cyclic voltammetry and electrochemical impedance spectroscopy. As shown in Fig. 1A, cyclic voltammograms on the different layers of the biosensor gave reversible peaks of the redox probe. The layers added to the surface caused significant changes to the cyclic voltammograms. The CV at the GCE, the GCE/Au, and the GCE/Au/Cys showed a well-defined electrochemical response for the redox probe. After the electrode was further modified with avidin, biotin, and VEGF-R1 the peak currents apparently decreased. This indicated that insulating layers of avidin, biotin, and of course, VEGF-R1 were introduced.

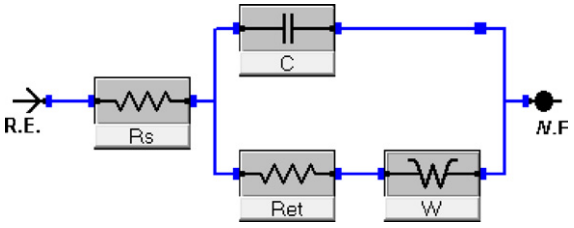

Fig. 2. Equivalent circuit model applied to fit the impedance measurements. R_s, the ohmic resistance of the electrolyte solution; C, associated with the double layer capacitance; R_{et}, the electron transfer resistance and W, the Warburg impedance.

Electrochemical impedance spectroscopy as Nyquist plots for the layer-by-layer assembly of the biosensor is shown in Fig. 1B. EIS is an advantageous method for exhibiting the characteristics of surface-modified electrodes [2,20,21]. The impedance spectrums show an increase in the electron transfer resistance (R_{et}) after each step of immobilization except for SAM formation of cysteamine, gold-plated GCE, and after EDC/NHS activation. R_{et} was the resistance which controlled the transfer of the redox probe through the electrode surface. There was an increase in R_{et} due to the attachment of proteins on the cysteamine-modified electrode. Moreover, since the formation of avidin–biotin complexes on the electrode surface increased the resistance of the surface, the impedance increased. The GCE electrode plated with gold had better conductivity than bare GCE. Because of this, the R_{et} value obtained for GCE/Au decreased. In the case of self-assembling of cysteamine which was positively charged, R_{et} was significantly decreased because of the electrostatic interaction between the positive amino group of cysteamine and the negatively charged redox probe. It can be concluded that a good linear relationship exists between semicircle diameters and electrode layers, which indicate successful construction of the biosensor. The electrochemical impedance data were fitted with an equivalent circuit model, shown in Fig. 2.

This equivalent circuit model consisted of resistive and capacitive elements, as well as a Warburg element. R_s was the resistance of the working solution, and the CPE (constant phase element) was connected with the capacitance of the complex bioactive layer. R_{et} was related to the electron transfer resistance through the electrode surface, and the Warburg impedance, Z_w, described the normal diffusion to the electrode surface through the complex layer.

In the present study, one of the most important issues was the immobilization procedure developed for VEGF-R1. First of all, the procedure used here provided a relatively long spacer arm for covalent binding of VEGF-R1 to the electrode. It is probable that the immobilization performance of VEGF-R1 was sterically enhanced by such a long spacer arm. Moreover, the same effect should have resulted in an increase in the binding percentage of VEGF to the VEGF-R1. In addition, the molecular oscillation obtained with a longer spacer arm was presumably higher than that obtained with a shorter arm. This molecular oscillation should make the diffusion of the redox probe, $K_4Fe(CN)_6/K_3Fe(CN)_6$, more sensitive to surface modifications, such as binding of VEGF to its receptor. Consequently, electrochemical impedance spectrums were affected by modifications of the electrode surface.

3.2. Optimization studies for VEGF-R1 immobilization

Layer-by-layer preparation of the VEGF-R1 biosensor was examined in terms of the incubation periods for biotin binding, VEGF-R1 binding, and VEGF/VEGF-R1 interaction. Details are given below.

In order to explain the effect of incubation time on the binding of biotin to avidin, three different incubation periods were tested for

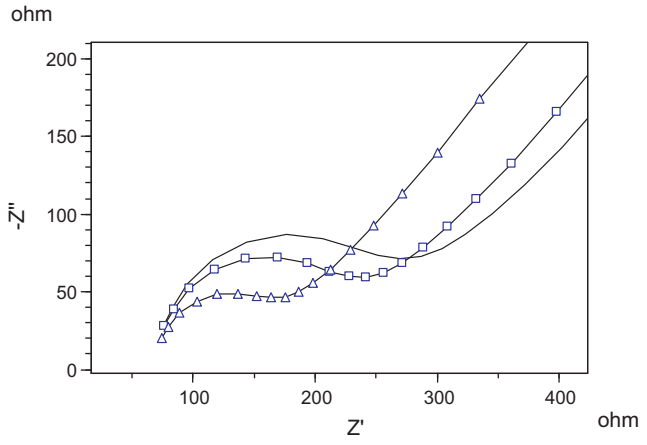

Fig. 3. The effect of biotin incubation period on immobilization performance. Electrochemical impedance spectrums obtained for different biotin incubation periods, -△-△-: incubation for an hour; -□-□-: incubation for 2 h; straight line: incubation for 4 h.

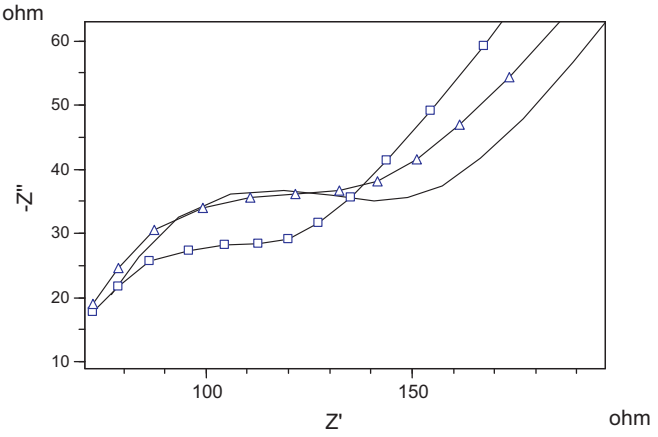

Fig. 4. The effect of VEGF-R1 incubation period on immobilization performance. Electrochemical impedance spectrums obtained for different VEGF-R1 incubation periods, -□-□-: incubation for an hour; -△-△-: incubation for 2 h; straight line: incubation for 4 h.

the performance of biotin binding. The electrochemical impedance spectrums of these studies are given in Fig. 3.

It can be seen that the binding of biotin to avidin was significantly affected by the incubation period. The peak currents were decreased by an increase in incubation times. This result was confirmed with the help of electrochemical impedance studies. The binding of biotin introduced an additional insulating layer on the avidin-modified surface, which increased the electron transfer resistance, implying a high impedance value (Fig. 3). The impedance values increased with the increase in incubation periods. The impedance values obtained for different incubation periods (1, 2 and 4 h) were 101.8, 158.4, 188.9 Ω, respectively. Further studies showed that a 2-h incubation period for biotin–avidin binding was efficient. As a result, in the following studies the avidin-modified electrode was incubated with a biotin solution for 2 h.

Another parameter was the incubation period for binding of VEGF-R1 to the activated –COOH terminal. The results of cyclic voltammograms indicated that there was a minor change in the peak current response of the redox probe when the incubation period was altered.

Meanwhile, the influence of the incubation period of VEGF-R1 on the performance of the biosensor was also investigated. The results are given in Fig. 4. When the electrode was incubated with the solution of VEGF-R1 for more than 2 h, there was almost no change in R_{et}. When the incubation period was less than 2 h, the R_{et} response decreased compared to the incubation periods of 2 and 4 h. The impedance values obtained for different incubation periods of VEGF-R1 (1, 2, and 4 h) were 48.7, 61.9, 71.7 Ω, respectively. As a result the best period for VEGF-R1 incubation was found to be 2 h.

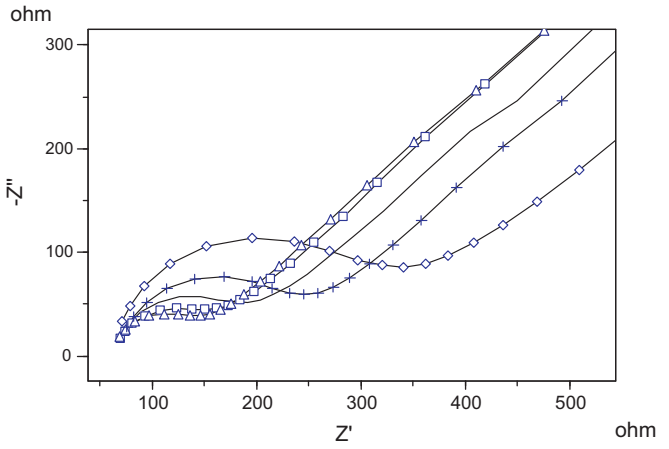

Fig. 5. Electrochemical impedance spectroscopy for the period of VEGF binding to the biosensor, -△-△-: incubation for 30 min, -□-□-: incubation period for 60 min; straight line: incubation for 2 h; -+-+-: incubation for 4 h; -◇-◇-: incubation for 6 h.

Eventually, the incubation period for binding between VEGF-R1 and VEGF was optimized. For this purpose, VEGF-R1/VEGF interaction was realized by using different incubation periods, such as 30 min, 1, 2, 4, and 6 h. The impedance spectrums can be seen in Fig. 5.

The binding ratio of VEGF to VEGF-R1 was increased by extending the incubation periods. This was due to the increase in binding performance of VEGF to VEGF-R1. Consequently the R_{et} values were increased by lengthening the period of incubation. The impedance values obtained for different incubation periods of VEGF binding (30 min, 1, 2, 4, and 6 h) were 79.3, 83.5, 110.5, 155, and 259.1 Ω, respectively. The total immobilization duration should be as short as possible, so taking all these factors into account the most effective period for VEGF incubation was determined to be 2 h. If VEGF-R1 and VEGF incubation periods are evaluated in terms of total measurement duration, short periods for both incubation processes are preferable.

3.3. Analytical characteristics of the biosensor

Fig. 6 shows the cyclic voltammograms and impedance spectrums obtained with the biosensor based VEGF-R1. From Fig. 6A, it can be seen that the peak values decreased with an increase in the VEGF concentration applied to the biosensor. As can be seen in Fig. 6B, an application of VEGF to the biosensor surface increased R_{et} values. This hindered the redox reaction of $[Fe(CN)_6]^{3-/4-}$ because an extra layer was formed on the surface. It is clear from the Nyquist plots that the low frequency ranges were particularly suitable for concentration-dependent impedance measurements.

The increment of VEGF concentration increased the charge transfer resistance, R_{et}, achieving a linear range between 100 fg mL^{-1} and 600 fg mL^{-1}. A calibration graph for VEGF was prepared with the help of the differences in charge transfer resistances after VEGF binding. The calibration curve is given in Fig. 7.

The change of charge–transfer resistance differences was calculated by the following equation:

$$\Delta R_{et} = R_{et(VEGF\text{-}R1/VEGF)} - R_{et(VEGF\text{-}R1)}$$

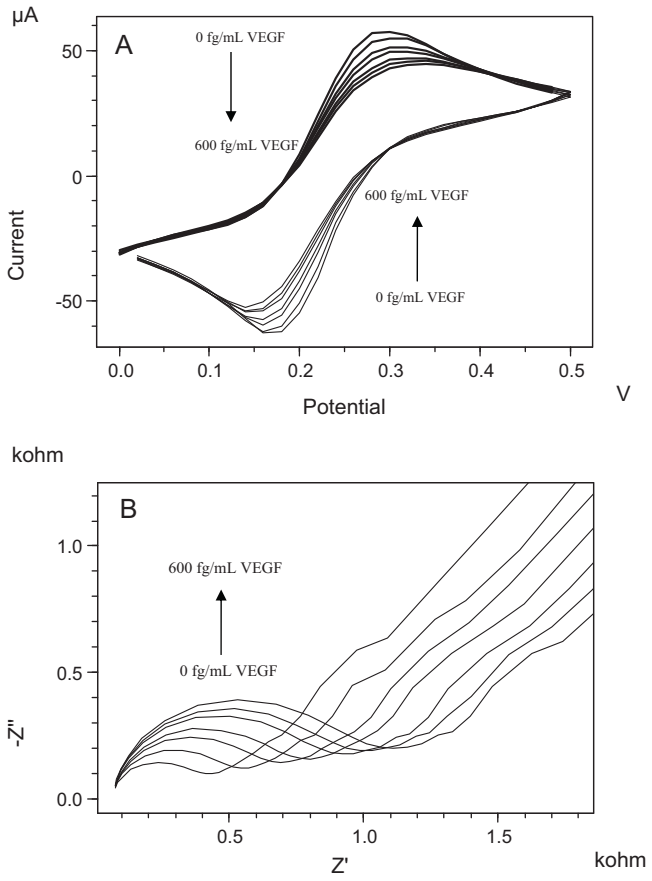

Fig. 6. Cyclic voltammograms (A) and impedance spectrums (B) obtained for different concentrations of vascular endothelial growth factor.

where $R_{et(VEGF\text{-}R1/VEGF)}$ is the value of the charge transfer resistance after VEGF-R1 is coupled to VEGF, while $R_{et(VEGF\text{-}R1)}$ is the value of the charge transfer resistance when VEGF-R1 was immobilized on the electrode.

In this study, the new biosensor system was also analyzed by Kramers–Kronig Transforms. The Kramers–Kronig relations are integral equations that constrain the real and imaginary components of complex quantities for systems that satisfy conditions of linearity, causality, and stability [22–24]. In principle, the Kramers–Kronig relations can be used to determine whether the impedance spectrum of a given system has been influenced by bias errors caused, for example, by instrumental artifacts or

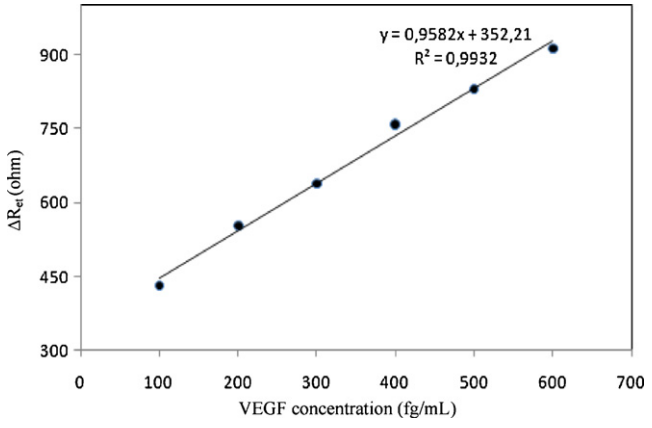

Fig. 7. VEGF calibration curve obtained by the biosensor based VEGF-R1.

Table 1
The results for Kramers–Kronig transforms, reproducibility, and the sample analysis.

Kramers–Kronig transforms for different layers of the biosensor

Biosensor surfaces	Goodness of fit values
GCE	9.461
GCE/Au	5.351
GCE/Au/Cys	8.239
GCE/Au/Cys/Avi	6.961
GCE/Au/Cys/Avi/Bio	5.690
GCE/Au/Cys/Avi/Bio/VEGF-R1	4.982
GCE/Au/Cys/Avi/Bio/VEGF-R1/VEGF	4.532

Reproducibility of the biosensor

Biosensor numbers	R^2	y	Linear ranges (fg mL^{-1})
1	0.9907	$1.2104x + 104.81$	100–600
2	0.995	$2.0122x + 167.71$	100–600
3	0.9932	$3.8327x + 352.21$	100–600
4	0.9895	$1.2344x + 123.14$	100–600
5	0.861	$1.0262x + 18.693$	100–600
6	0.8446	$0.3978x + 54.907$	100–600
7	0.948	$0.4834x + 17.767$	100–600
8	0.9725	$0.4072x + 42.52$	100–600
9	0.9949	$0.6223x + 56.133$	100–600

VEGF detection in artificial serum samples

VEGF (fg mL^{-1})			
Added	Found by the biosensor	% Recovery	% Relative difference
100	104.5	104.5	4.5
200	211.6	105.8	5.8
400	415.8	103.95	3.95

time-dependent phenomena [24]. The Kramers–Kronig relations have been applied to electrochemical systems by direct integration of the equations, by experimental observation of stability and linearity, by regression of specific electrical circuit models, and by regression of generalized measurement models [25,26]. Direct integration of the Kramers–Kronig relations involves calculating one component of the impedance from the other, e.g., the real component of impedance from the measured imaginary component. The result is compared to the experimental values obtained [24].

In this study, Kramers–Kronig Transforms were performed using software produced by Gamry Instruments Inc. (Gamry Instruments Inc., USA). Calculations were carried out following the method of Boukamp [27].

According to these calculations, a value named "Goodness of Fit" was obtained. In addition, a plot of the relative errors ($\Delta Z/Z$) for the real and imaginary parts of the experimental data was also drawn. For the present new biosensor, for all steps including preparation of the biosensor and measurement, Kramers–Kronig Transforms were performed. The goodness of fit values of different biosensor surfaces are also given in Table 1.

The Kramers–Kronig transforms performed on the electrochemical impedance spectrums related to the biosensor revealed that the experimental data agreed with the data obtained by the transforms. Nevertheless it was very important that the impedance spectrums were linear, stable, and formed a causal circuit. Finally, it was also important that the system was not influenced by unknown variables.

The charge transfer resistances of the biosensor were investigated when it was consecutively exposed to a 200 fg mL^{-1} VEGF standard solution nine times. The repeatability of the measurements was very good considering that the correlation coefficient of measurements was 1.95%, and the average value and standard deviation were calculated as 203.3 fg mL^{-1} and ±3.96 fg mL^{-1},

respectively. The results showed that the biosensor exhibited a fairly desirable analytical feature of repeatability. The reproducibility of the same nine biosensors was also examined. For this purpose, nine biosensors were assembled in the same way with different bare glassy carbon electrodes.

The linear detection ranges of all nine biosensors were the same as 100–600 fg mL^{-1}. The results of the reproducibility studies are given in Table 1. The biosensor described here also provided excellent reproducibility. The results are again summarized in Table 1.

To illustrate the feasibility of the biosensor in practical analysis, artificial serum samples were prepared by the addition of VEGF standard solutions. These artificial serum samples were analyzed using the proposed impedimetric biosensor based on VEGF-R1. As shown in Table 1, the good recoveries in the ranges of 103.95–105.8% were obtained. This indicated that the presented biosensor might be useful for the analysis of VEGF in real clinical samples.

4. Conclusion

In conclusion, we have successfully developed a novel and efficient biosensor utilizing vascular endothelial growth factor receptor-1 as a bioreceptor for the diagnosis of vascular endothelial growth factor. The detection of the target protein, VEGF was successfully made at the femtogram mL^{-1} range. The immobilization method demonstrated herein introduced an ultra sensitive biochemical matrix as well as a very useful way to bind a bioreceptor to the electrode surface. The biosensor utilizing VEGF-R1 as a biorecognition element showed an excellent affinity to its ligand, VEGF, with good linearity for VEGF determination in a range of 100–600 fg mL^{-1}. The repeatability and reproducibility of the biosensor were also good. The Kramers–Kronig transforms revealed that the whole biosensor system was linear, stable, and formed a causal circuit. This meant that the biosensor system was not influenced by unknown variables. Also, in the method presented here, VEGF was detected more sensitively than with the other methods mentioned above. Moreover the detection limit of the biosensor was 100 fg mL^{-1} for VEGF. This limit was the best one of all VEGF detection methods discussed here. Moreover, the construction procedure for the biosensor was very simple, and it could be used in almost all biosensor laboratories for novel biosensor development.

Acknowledgment

The authors are grateful to TÜBİTAK (The Scientific and Technological Research Council of Turkey, Project number: 109T 172) for supporting this research.

References

[1] A.W. Bott, Curr. Sep. 19 (2001) 71–75.
[2] E. Katz, I. Willner, Electroanalysis 15 (2003) 913–947.
[3] J.G. Guan, Y.Q. Miao, Q.J. Zhang, J. Biosci. Bioeng. 97 (4) (2004) 219–226.
[4] Y. He, S.K. Smith, K.A. Day, D.E. Clark, D.R. Licence, D.S. Charnock-Jones, Mol. Endocrin. 13 (4) (1999) 537–545.
[5] B. Olofsson, E. Korpelainen, M.S. Pepper, S.J. Mandriota, K. Aase, V. Kumar, Y. Gunji, M.M. Jeltsch, M. Shibuya, K. Alitalo, U. Eriksson, Proc. Natl. Acad. Sci U.S.A. 95 (20) (1998) 11709–11714.
[6] G. Conn, D.D. Soderman, M.T. Schaeffer, M. Wile, V.B. Hatcher, K.A. Thomas, Proc Natl. Acad. Sci. U.S.A. 87 (4) (1990) 1323–1327.
[7] Y. Amo, M. Masuzawa, Y. Hamada, K. Katsuoka, Br. J. Dermatol. 150 (1) (2004) 160–161.
[8] E. Liu, M. Morimoto, S. Kitajima, T. Koike, Y. Yu, H. Shiiki, M. Nagata, T. Watanabe, J. Fan, J. Am. Soc. Nephrol. 18 (7) (2007) 2094–2104.
[9] H.R. Byon, H.C. Choi, J. Am. Chem. Soc. 128 (2006) 2188–2189.
[10] Y. Cui, Q. Wei, H. Park, C.M. Lieber, Science 293 (17) (2001) 1289–1292.
[11] Z. Gao, A. Agarwal, A.D. Trigg, N. Singh, C. Fang, C.-H. Tung, Y. Fan, K.D. Buddharaju, J. Kong, Anal. Chem. 79 (2007) 3291–3297.
[12] J. Hahm, C.M. Lieber, Nano Lett. 4 (2004) 51–54.
[13] A. Kim, C.S. Ah, H.Y. Yu, J.-H. Yang, I.-B. Baek, C.-G. Ahn, C.W. Park, M.S. Jun, S. Lee, Appl. Phys. Lett. 91 (2007) 103901.
[14] F. Patolsky, G. Zheng, O. Hayden, M. Lakadamyali, X. Zhuang, C.M. Lieber, Proc. Natl. Acad. Sci. U.S.A. 101 (2004) 14017–14022.
[15] E. Stern, J.F. Klemic, D.A. Routenberg, P.N. Wyrembak, D.B. Turner-Evans, A.D. Hamilton, D.A. LaVan, T.M. Fahmy, M.A. Reed, Nature 445 (2007) 519–522.
[16] H.-S. Lee, K.S. Kim, C.-J. Kim, S.K. Hahn, M.H. Jo, Biosens. Bioelectron. 24 (6) (2009) 1801–1805.
[17] S. Prabhulkar, S. Alwarappan, G. Liu, C.-Z. Li, Biosens. Bioelectron. 24 (12) (2009) 3524–3530.
[18] B. Lu, J. Xie, C. Lu, C. Wu, Y. Wei, Anal. Chem. 67 (1) (1995) 83–87.
[19] G. Kim, K.-W. Kim, M.-K. Oh, Y.-M. Sung, Biosens. Bioelectron. 25 (2010) 1717–1722.
[20] A.B. Kharitonov, L. Alfonta, E. Katz, I. Willner, J. Electroanal. Chem. 487 (2001) 133–141.
[21] D. Tang, R. Yuan, Y. Chai, J. Dai, X. Zhong, Y. Liu, Bioelectrochemistry 65 (2004) 15–22.
[22] R. de, L. Kronig, J. Opt. Soc. Am. Rev. Sci. Inst. 12 (1926) 547–557.
[23] H.A. Kramers, Phys. Z. 30 (1929) 522–523.
[24] E.M. Orazem, B. Tribollet, Electrochemical Impedance Spectroscopy, A John Wiley & Sons, NJ, 2008.
[25] Q.-A. Huang, R. Hui, B. Wang, J. Zhang, Electrochim. Acta 52 (2007) 8144–8164.
[26] W. Ehm, H. Gohr, R. Kaus, B. Roseler, C.A. Schiller, ACH Models Chem. 137 (2000) 145–157.
[27] B.A. Boukamp, J. Electrochem. Soc. 142 (1995) 1885–1894.